Inflation of ponded, particulate laden, density currents.

ROBERT M. DORRELL,[1*] MARCO PATACCI[2] and WILLIAM D. MCCAFFREY[2]

[1] Energy and Environment Institute, University of Hull, Hull, UK

[2] School of Earth and Environment, University of Leeds, Leeds, UK

[*] corresponding author r.dorrell@hull.ac.uk

KEYWORDS

Turbidity Currents

Ponded Flows

Seafloor Basins

Inflation

Deposits

The published version is available at https://pubs.geoscienceworld.org/sepm/jsedres/article/88/11/1276/566309/Inflation-of-Ponded-Particulate-Laden-Density

ABSTRACT

Field-based, physical modelling and analytical research approaches currently suggest that topographically confined particle-laden density currents commonly inflate to produce suspension clouds that generate tabular and texturally homogeneous sedimentary deposits. Here, a novel three-dimensional theoretical model details a phase space of the criteria for inflation as a function of flow duration, basin size and geometry, total mass transport, sediment concentration, and particle grain size. It shows that under most circumstances cloud inflation is unlikely at real-world scales. Even where inflation is possible, inflation relative to initial flow height is small except for suspensions of silt or finer-grained sediment. Tabular deposits therefore either arise from processes other than flow ponding, or deposits in confined settings may be significantly more complex than are currently understood, due to processes of autogenic compensation and channelization, with associated implications for reservoir characterisation in applied contexts. This study illustrates the potential of analytical flow modelling as a powerful complement to other research approaches.

INTRODUCTION

Density currents driven by suspended particulate material are a key mechanism for atmospheric, fluvial, and marine sediment transport. In natural or artificial basins, these flows are trapped by confining slopes and become ponded (Van Andel and Komar 1969). Key examples include hyperpycnal inflow into lakes, reservoirs, and small seas; turbidity-current inflow into bathymetric lows; and topographically confined snow or dust storms. If supply of material into a ponded flow exceeds that lost through deposition, and/or overspill, the ponded flow thickens and forms an inflating cloud eventually, filling the confining basin (Lamb et al. 2004, Toniolo et al. 2006). This process is limited only if outflow balances inflow, where a quasi-steady cloud is established (Patacci et al. 2015). If the outflow exceeds inflow, then the volume of the ponded cloud decreases.

A common feature of confined deep-water basins is the deposition of apparently tabular deposits, attributed to basin fill by ponded turbidity currents (e.g., Twitchell et al. 2005). Inflation of ponded turbidity currents is thought to produce homogeneous clouds of suspended particulate material, and thus basin-wide tabular deposits (Toniolo et al., 2006; Sylvester et al., 2015). Models of turbidite sand pinchout geometry commonly show conceptual tabular geometries for the sands remote from the confining slope (Smith and Joseph, 2004; Gardiner, 2006; Bakke et al., 2013; Spychala et al., 2017). Hydrocarbon reservoirs can be hosted in such deposits, with the degree of deposit homogeneity on the basin floor and the extent of sand deposited on the confining slopes being key factors that dictate their economic significance (Amy et al., 2013). Therefore, it is important to understand controls on deposit formation in confined settings. Here we use a novel mass-conservation model to produce computational stratigraphy, assessing the role of topographic confinement on flow ponding and inflation and thereby evaluating the likely character of associated sedimentary deposits.

METHODS

For density currents to pond and inflate they must first traverse their confining basin. Traverse times can be estimated by the fluid input rate into the basin, q_I, and three-dimensional basin geometry. The flow input rate into the basin is given by

$$q_I = \begin{cases} \frac{M}{\rho_s C t_d} & t \leq t_d \\ 0 & \text{otherwise} \end{cases}, \qquad (1)$$

where M is the total mass of sediment transported into the basin; C is the suspended-sediment concentration; ρ_s is the sediment density; and time $t = t_d$ is the flow duration, denoted by subscript d notation. For simplicity, the model is constrained to well-mixed flows, where C is approximately constant for the duration of the flow. A generic basin is considered (Fig. 1), where sidewall slopes, S_1 to S_4, and basin-floor length, L, and width, W, scales can vary independently. However, over the course of a single flow, change in basin bathymetry, η, is assumed negligible in comparison to initial basin length scales. The plan-form area, A, cross-sectional area, B, and volume, V, of the ponded flow are thus a function of flow depth, H.

Entering the basin, the flow is assumed to expand rapidly to the sidewall width, W. This assumption provides a first-order estimate of the flow dynamics, where depositional heterogeneities that may be formed in the developing flow near the inlet are omitted. However, it does not affect the conditions for ponded cloud inflation and simplifies the physical processes to a tractable form as discussed below. The initial flow traversing the basin floor is denoted by subscript t notation, i.e., depth $h_t = H_t$ and average velocity U_t. Net deposition and entrainment are initially assumed negligible (Hogg et al., 2015). The velocity on the basin floor is given by the Froude number condition, $Fr = U_t/\sqrt{gRCH_t}$, where R is the reduced density $R = \rho_s/\rho - 1$. Initial flow depth is therefore defined implicitly by the discharge, as equal to the product of flow velocity and cross-sectional area,

$$q_I = Fr\sqrt{gRCH_t}B_t. \tag{2}$$

For fixed discharge the depth of the flow traversing the basin, H_t, decreases with increasing Froude number. The Fr of a density-current head decreases with flow-ambient fluid depth ratio. Here we assume the limit of an infinitely deep ambient and take the Froude number of the flow as it traverses the basin as equal to unity, $Fr = 1$ (Shin et al., 2004). The time taken for a flow to cross a basin, and fill it to height H_t, is $t_t = V_t/q_I$. From Equation 2, increasing the front Froude condition has the effect of reducing the time taken, t_t, and the depth of the flow, H_t, whilst the flow traverses the basin. On crossing the basin, the flow may run up the distal slope, exchanging kinetic energy for potential energy. An energy balance yields the maximum run-up height of the flow, denoted by subscript r,

$$H_r = H_t\left(1 + \frac{Fr^2}{2}(1 - E)\right), \tag{3}$$

where $E = 33\%$ is the energy lost to thermal dissipation (Allen, 1985). Equation 3 is a lower limit on the flow run-up height, which may be enhanced as the center of gravity of the flow changes as it runs up the slope (Muck and Underwood, 1990).

After the flow has traversed the basin, mass conservation of the suspended sediment, settling with velocity w_s (Soulsby, 1997), predicts the inflation of the now ponded flow. Simply, the time rate of change in the volume-integrated suspended-sediment concentration, VC, is given by the inflow of sediment-laden fluid into the basin, $q_I C$, minus the area-integrated rate of sediment deposition, ACw_s, and overspill of sediment-laden-fluid, $q_o C$. Following a similar argument, the change in bed depth, η, is the rate of deposition divided by the change in concentration between the bed, $C_m = 0.6$, and the suspension (Dorrell and Hogg, 2010). Therefore, mass conservation yields two equations for the evolution of the ponded cloud and deposit, decoupled under the assumption that change in basin bathymetry is negligible for a single flow (see supplementary material),

$$\frac{d}{dt}VC = q_I C - ACw_s - q_O C, \tag{4a}$$

$$\frac{d\eta}{dt} = \begin{cases} Cw_s/(C_m - C) & \eta < H \\ 0 & \text{otherwise} \end{cases}. \tag{4b}$$

For simplicity, the hydrodynamic characteristics and sediment composition of the flow entering the basin are assumed constant in time. Further, sediment is assumed to be kept in suspension by turbulent diffusion (Dorrell et al., 2013), driven by the continuous flow into the basin. Suspension may be enhanced by the upflow of fluid in the inflating ponded cloud. Thus, as a first-order approximation, particulate material in suspension is assumed unstratified as the ponded cloud inflates; significant stratification is assumed to develop only once the flow into the basin is extinguished. As the flow is assumed unstratified, C is constant. However, variations in area and volume-averaged, inflow and outflow concentration in a stratified flow are analogous to variations in the inflow and outflow discharge and settling velocity. Here inflation is modeled for confined flows, $q_o = 0$, although overspill acts as a hard limit on cloud inflation (Toniolo et al., 2006). As V is the depth integral of A, then ponded-cloud inflation (Eq. 4a) is simplified to an integral equation

$$\int_{H_t}^{H} \frac{A}{q_I - Aw_s} dH = \int_{t_t}^{t} dt. \tag{5}$$

Whilst inflow discharge is greater than the rate of detrainment, the height of the ponded cloud increases in time.

Eventually the inflating cloud tends to an equilibrium, denoted subscript e, where input and detrainment balance,

$$q_I = A_e w_s. \quad (6)$$

For $t_t \leq t < t_e$ Equation 5 has exact solutions (see supplementary material) that define ponded cloud inflation height, H, at time t. However, as the ponded-cloud volume increases, the rate of change of volume monotonically decreases to zero, (Eq. 4a). Therefore, $H \to H_e$ is reached only at time $t_e \to \infty$. This limit is a consequence of inflation limited by the growth of the detrainment surface area, A, with flow depth.

RESULTS

In Figure 2A ponded-cloud inflation rate, derived from Equation 5, compares well to experiments of topographically confined turbidity currents (see experiment L6 Patacci, 2010; Patacci et al. 2015). The experiments were conducted in a two-dimensional basin, of rectangular cross section, that was 5.12 m long, 0.35 m wide and 0.35 m and deep The basin was situated in a tank of 0.8 m ambient fluid depth. Sediment used in the experiments consisted of tightly distributed fine-grained 40 μm ballotini (non-cohesive, nearly spherical glass beads). To account for flow-ambient fluid mixing at the inlet, experiment L6 of Patacci (2010) is characterized by the recorded depth, velocity, and density of the flow as it traversed the basin, and by the duration of the flow t_d = 590 s. The average height of the experimental flow as it traversed the basin was H_t = 0.1m. The flow had a front velocity U_t = 0.1 m s^{-1}; width and depth integration of the front velocity yields the effective inlet discharge, $q_I = 3.6\times10^{-3}$ m^3 s^{-1}. The total mass of sediment transported into the basin, M = 39.4 kg, particle density ρ_s = 2650 kg m^{-3}, and the total fluid discharge, $q_I \times t_d$, defines the effective flow concentration, $C = 0.7\%$, Equation 1. The calculated experimental flow-front Froude number was 0.93.

Comparison of model to experimental flow inflation is made using a clearly defined dense layer visible in the experiments (Patacci et al. 2015). Above this dense layer, there is a comparatively thin dilute suspension cloud. This dilute suspension cloud is generated by mixing of the suspension and ambient fluid entrainment, driven by flow reflection off the distal slope (Patacci et al. 2015). As this layer is dilute, it is assumed of negligible importance (Patacci, 2010; Patacci et al. 2015); thus it is assumed that the experiment is well described by the entrainment-free model, Equation 4. Predicted rates of inflation are slightly greater than that observed. This can be explained by a component of mass loss through overspill, as the distal experimental basin slope was of limited height, possibly augmented by subtle stratification effects in the lower dense layer (Patacci et al., 2015).

The inflation of a ponded flow, Equation 5, can be parametrized by three key dimensionless variables:

$$\frac{q_I}{WLw_s},\ \frac{w_s t_d}{H_t},\ \text{and}\ \frac{t_t}{t_d}, \qquad \text{(7a-c)}$$

respectively: the ratio of inflow discharge to the rate of deposition across the initial basin area (Eq. 7a); and the ratio of settling velocity to flow depth over flow duration (Eq. 7b). Initial conditions are prescribed by the ratio of run-out time to flow duration (Eq. 7c). Inflation is also dependent on basin geometry; the dimensionless parameters of basin width to length and slope aspect ratios determine how quickly solutions tend towards equilibrium flow height (Fig. 2B). However, not all ponded flows have sufficient discharge or are of sufficient duration to inflate; for example, some flows may only just reach and reflect off the distal basin slope before collapsing (i.e., reflected surge flows: Komar, 1977; Patacci et al., 2015). A necessary, but not sufficient, criterion to distinguish inflating clouds, and in particular their deposits, from other ponded flows is that cloud depth, H, exceeds the run-up height of the flow, H_r, after it first traversed the basin; here the case $H > H_r$ is referred to as substantial inflation. For flows of nearly infinite duration (such as hyperpycnal inflow into lakes, reservoirs and small seas) this is simplified to $H_e > H_r$ (Fig. 2C). From Equation 5 it is seen that this is satisfied only if inflow discharge is greater than detrainment at the run-up height H_r, $q_I > A_r w_s$. Change in basin geometry significantly affects this criterion. For example, wider basins are traversed by shallower flows and are thus more likely to inflate (Fig. 2C). Further, the criterion $H_e > H_r$ scales linearly with H_r in two-dimensional basins. However, even in steep-sided three-dimensional basins the inflation criterion scales quadratically with H_r (Fig. 2C). This is because basin area $A = (L +$

$2S_L H)(W + 2S_W H)$ is quadratic in H, where average inverse slopes $S_L = \frac{1}{2}\left(\frac{1}{S_1} + \frac{1}{S_2}\right)$ and $S_W = \frac{1}{2}\left(\frac{1}{S_3} + \frac{1}{S_4}\right)$ are non-zero.

For finite flows, of duration $t = t_d$, the maximum height of the inflated cloud is denoted $H(t_d) = H_d$. The condition for substantial inflation, $H_d > H_r$, is given by the criteria that: i) flow duration must be sufficient for the flow to traverse the basin, $t_d > t_t$; and ii) [that] the inflow discharge is greater than detrainment at run-up height, $q_I > A_r w_s$. If inflow discharge, or flow duration, is decreased, inflation of ponding flows may be reduced or become impossible; see Table 1. For example: if inflow discharge is less than detrainment at initial flow height, but greater than that on the basin floor, LWw_s, the flow ponds but does not inflate; if flow duration is less than the time taken to cross the basin the “surge flow” does not inflate but reflects off the basin slope(s) until dissipated (Komar, 1977); or if detrainment across the basin floor is greater than the inflow discharge, then the accommodation space is too large for ponding and the flow is effectively unconfined.

Based on the inflation model, Equation 4, Figure 3 plots the phase space of the scenarios in which real-world-scale ponded flow may inflate, and the flow inflation relative to initial height, as a function of basin geometry (Fig. 3A-C) and ponded-flow makeup (Fig. 3D-F). For each plot, flow duration and one other parameter are varied, while all other variables are kept constant. Flow duration is kept as a free variable, because it is the least well constrained parameter for which a reasonable average value can be estimated. The fixed values describe: a relatively small ($LW = 100$ km^2), equant ($W/L = 1$ m/m) and steep-flanked ($S_1 = 0.1$ m/m = 5.74 degrees) basin; a low-concentration flow (depth-average concentration, $C = 0.3\%$), composed of fine sand ($d = 177$ μm); and sufficient sediment transported to generate a deposit 6.4 m thick if uniformly distributed across the basin floor, $M/LW = 10$ tonnes m^{-2}. These parameters were chosen because they represent real-world scenarios where inflation would be expected, i.e., a very large fine-grained flow entering a small basin with steep flanks. In addition, the inflation estimates shown in Figure 3 are optimistic, in that they may be limited by overspill in real-world settings (Pirmez et al., 2012). Plots of calculated basin-floor deposit thickness, absolute inflation heights, and the time taken by the flow to traverse the basin are provided in the supplementary material. Basin-geometry and ponded-flow variables are contrasted to characteristic basin geometries and deposit and turbidity-current conditions from ancient and modern deep-water systems; see white arrows in Figure 3 and Table 2 for original data sources.

Figure 3A shows that for medium to small basins (e.g., Brazos IV, BR), there is limited inflation above the run-up height of the flow. In large basins (e.g., Marnoso-Arenacea, MA) the ability to inflate the ponded cloud decreases. Moreover, only large events (leaving a deposit > 1 m thick) transport enough mass per basin area to cause any inflation, with inflation of the larger events (depositing beds 5 to 20 m thick) limited to 1.5-2.0 times the original thickness of the flow (Fig. 3D). Figure 3E shows that values of depth-averaged sediment concentration in the range 0.05-0.5%, typical of observed turbidity currents, lead to the largest inflation. However, such inflation is again limited compared to the run-up height of the flow, suggesting that ponded deposits may be difficult to distinguish from surge-flow deposits in the rock record. Inflation is more significant in wider basins (Fig. 3B) and in the case of steeper confining slopes (Fig. 3C). However, basins with very steep slopes (> 10°) or that have a high width-to-length aspect ratio (> 2), where the flow width is comparable to the basin width, represent very uncommon scenarios. Therefore, the general conclusion from Figure 3 is that in real-world scenarios for sandy flows traversing a basin, inflation past the run-up height is constrained to a small area of the phase space, and that any inflation that does occur within the duration of the flow is small in comparison to the height of the flow as it travels across the basin floor.

The exception to the general conclusion that ponded clouds do not inflate significantly beyond 1.5 times the predicted depth of the flow in the basin (see Fig. 3) is for flows of finer particle size; here quadratic decrease in settling velocity significantly enhances the potential flow inflation for silty and muddy flows (Fig. 3F). This suggests that in polydisperse flows, inflation heights of different grain sizes are decoupled, providing a means to cause planform grain-size fractionation in deposits.

DISCUSSION

The analytical model presented here suggests that turbidity currents are unlikely to form ponded sandy clouds in confined basins under most circumstances. Sandy deposits in confined basins are therefore unlikely to form beneath such clouds, and this scenario of deposition can be recognized as only one of four distinct interaction styles of turbidity current with confining bathymetry (Table 1, Fig. 3G). It can be postulated that each likely has its own depositional signature:

i) Turbidity currents inflate to fill a basin, producing tabular beds that extend across the entire basin (Fig. 4A). Although substantial inflation of the sandy component of ponded clouds in confined basins is considered unlikely under the broad range of realistic scenarios of flow conditions, basin geometries and deposits considered, tabular deposits that may have formed under such conditions include the Lower and Middle Fans / Series 20 and 40 (*sensu* Beauboeuf et al., 2003 and Prather et al., 2012, respectively) of Basin IV of the Brazos-Trinity slope system, western Gulf of Mexico); these deposits can be imaged in relatively high detail using high-frequency 3D seismic data. Outcropping systems provide only quasi-3D control on bed geometry at best. Nevertheless, tabular beds in confined basins, e.g., the Castagnola system of northern Italy (Marini et al., 2016), can be considered candidates to have formed beneath sandy suspensions.

ii) Ponded turbidity currents may extend across the whole basin, but do not inflate. The architectural style of associated deposits may vary significantly. Deposition from a current reflected off the confining slopes may induce tabularity; in this case paleocurrent data, where available, might indicate variable paleoflow orientations (Haughton 1994, 2001; Amy et al., 2007; Tinterri and Tagliaferri, 2015). With flows that ran parallel to the long axis of a thin basin, the Tabernas-Sorbas system is a candidate for such depositional types (Fig. 3B). Alternatively, beds might taper distally, and possibly show subtle autogenic stacking effects (Fig. 4B), for example the Upper Fan / Series 70 perched apron (*sensu* Beauboeuf et al., 2003 and Prather et al., 2012, respectively) of Brazos-Trinity Basin IV.

iii) Turbidity currents are of insufficient duration to fill the basin. In this case, individual current characteristics will determine the *loci* of deposition; sequences of similar currents might produce ordered, compensationally stacked lobes (Deptuck et al., 2008, MacDonald et al., 2011, Prelat and Hodgson, 2013), whereas flows of varying character could produce disordered deposits (Fig. 4C).

iv) Turbidity currents end within the basin, possibly, though not necessarily interacting with lateral topography. Associated deposits are likely to show autogenic effects in their architecture, including lobe compensation and channelization (Fig. 4D). Such deposits are likely to conform to the style of unconfined lobes, which are described by an extensive literature (e.g., Deptuck et al., 2008, MacDonald et al., 2011, Prelat and Hodgson, 2013).

Analytical modelling provides new constraints on the likelihood of inflation of ponded turbidity currents, suggesting that a range of flow processes and depositional products is likely in confined settings. A consequence is that the stratigraphic architecture generated by confined flows is likely much more complex than previously thought; sandy deposits in confined basins are unlikely to form from inflated ponded clouds and therefore could be tabular for another reason, or more heterogeneous in their planform distribution (Figs. 3, 4). Future work is needed to explore the dynamics and relative likelihoods of the extended range of interaction styles postulated. Theoretically based flow models offer a new means to test and upscale the results from complementary experimental models, to provide better constraint on the interpretation of field scale observations of sedimentary architecture. The present model, however, does not take flow grain size or density stratification into account and cannot therefore realistically predict bed pinchout geometries, including the height to which turbidites drape slopes. Both outcrop and seismic case studies suggest that different grain size fractions in a flow may pond to different heights (Badalini et al., 2000; McCaffrey and Kneller, 2001, Smith and Joseph, 2004, Twichell et al., 2005; Gardiner, 2006). To provide a better-calibrated constraint on the dynamics and relative likelihoods of the range of interaction styles of ponded flows with their confining bathymetry, the model should be extended to incorporate stratification effects.

CONCLUSIONS

Deposits confined gravity current in, for example, seafloor mini-basins are commonly modelled as being nominally tabular. A potential mechanism to generate such tabularity is the inflation of ponded gravity currents in the basin to produce a homogeneous suspension from which the deposits are ultimately formed. Here we discuss the conditions for ponded-cloud inflation and use a simplified mass-conservation model to show that substantial inflation of ponded flows is unlikely in real-world basins where: i) three-dimensional variations in basin geometry increase the detrainment surface area rapidly with increasing ponded-cloud depth; ii) detrainment in real-world scenarios is much greater than expected sediment supply; and iii) flows are of insufficient duration to traverse the basin before their supply into the basin is extinguished. The exception to this general rule is the inflation of gravity currents dominated by fine-grained sediments, where detrainment decreases quadratically with particle size. From the mass-conservation model we are able to investigate a phase space of basin and flow conditions where ponded currents may inflate. We also delimit the various regions where inflation is impossible, where the source flow either deflates through detrainment, is of insufficient duration to traverse the basin (i.e. reflected surge flows) or is effectively unconfined. The modelled case study suggests that deposit tabularity either arises for a reason other than sedimentation from an inflated suspension cloud, or that basin fill may be more heterogeneous than commonly modelled. Linking analytical modelling of flow dynamics and deposit structure (tabularity in this case) is demonstrated to be a technique complementary to experimental modelling and analysis of field data.

ACKNOWLEDGEMENTS

This research was funded by the Turbidites Research Group sponsors: AkerBP, BP, ConocoPhillips, ENI, Hess, Murphy, OMV, Shell and Statoil. Rufus Brunt, Matthieu Cartigny, Joris Eggenhuisen, Roberto Tinterri, and Matthew Wolinsky are thanked for providing thought-provoking reviews on the manuscript that have significantly improved it.

REFERENCES CITED

ALLEN, J.R.L., 1985, Principles of Physical Sedimentation, Chapter 12: London, George Allen and Unwin, p. 223-242.

Amy, L.A., McCaffrey, W.D. and Kneller, B.C., 2007, The Peira Cava Outlier, Annot Sandstones, France, in Nilsen, T.H., Shew, R.D., Steffens, G.S. and Studlick, J.R.J. eds., Atlas of Deep-Water Outcrops: American Association of Petroleum Geologists, Studies in Geology 56, p. 185-187.

Amy, L.A., Peachey, S.A., Gardiner, A.R., Pickup, G.E., Mackay, E., and Stephen, K.D., 2013, Recovery efficiency from a turbidite sheet system: numerical simulation of waterflooding using outcrop-based geological models: Petroleum Geoscience, v. 19, p. 123-138.

Argnani, A., and Ricci Lucchi, F., 2001, Tertiary silicoclastic turbidite systems of the Northern Apennines, in Vai, G.B., and Martini, I.P., eds, Anatomy of an Orogen: The Apennines and Adjacent Mediterranean Basins: Springer Netherlands, p. 327-349.

Badalini, G., Kneller, B.C., and Winker, C.D., 2000, Architecture and Processes in the Late Pleistocene Brazos-Trinity Turbidite System, Gulf of Mexico, Continental Slope: [in] Gulf Coast Section of the Society for Sedimentary Geology Foundation 20th, Annual Research Conference, Deep-Water Reservoirs of the World, p. 16-34.

Bakke, K., Kane, I.A., Martinsen, O. J., Petersen, S. A., Johansen, T. A., Hustoft, S., Jacobsen, F. H. and Groth, A., 2013, Seismic modeling in the analysis of deep-water sandstone termination styles: American Association of Petroleum Geologists Bulletin, v. 97, p. 1395-1419.

Beaubouef, R.T., Abreu, V., and Van Wagoner, J.C., 2003, Basin 4 of the Brazos-Trinity slope system, western Gulf of Mexico: The terminal portion of a late Pleistocene lowstand systems tract, in Roberts, H.H., Rosen, N.C., Fillon, R.H. and Anderson, J.B. eds., Gulf Coast Section of the Society for Sedimentary Geology Foundation, 23rd Annual Research Conference, Shelf Margin Deltas and Linked Down Slope Petroleum Systems: Global Significance and Future Exploration Potential, p. 45-66.

Carter, L., Milliman, J.D., Talling, P.J., Gavey, R., and Wynn, R.B., 2012, Near-synchronous and delayed initiation of long run-out submarine sediment flows from a record-breaking river flood, offshore Taiwan: Geophysical Research Letters, v. 39, no. L12603.

Cooper, C., Wood, J., and Andrieux, O., 2013, Turbidity current measurements in the Congo Canyon, in Annual Offshore Technology Conference, Proceedings of the OTC 23992.

Deptuck, M.E., Piper, D.J.W., Savoye, B., and Gervais, A., 2008, Dimensions and architecture of late Pleistocene submarine lobes off the northern margin of East Corsica: Sedimentology, v. 55, p. 869-898.

Dorrell, R.M., and Hogg, A.J., 2010, Sedimentation of bidisperse suspensions: International Journal of Multiphase Flow, v. 36, p. 481-490.

Dorrell, R.M., Hogg, A.J., and Pritchard, D., 2013, Polydisperse suspensions: Erosion, deposition, and flow capacity: Journal of Geophysical Research - Earth Surface, v. 118, p. 1939-1955.

Expedition 308 Scientists, 2006, Site U1320, in Flemings, P.B., Behrmann, J.H., John, C.M., and the Expedition 308 Scientists, Proceedings of the Integrated Ocean Drilling Program, 308: College Station Texas.

Felletti, F., 2002, Complex bedding geometries and facies associations of the turbiditic fill of a confined basin in a transpressive setting (Castagnola Fm., Tertiary Piedmont Basin, NW Italy): Sedimentology, v. 49, p. 645-667.

Gardiner, A.R., 2006, The variability of turbidite sandbody pinchout and its impact on hydrocarbon recovery in stratigraphically trapped fields, in Allen, M.R., Goffey, G.P., Morgan, R.K. and Walker, I.M. eds., Deliberate Search for the Stratigraphic Trap: Geological Society of London Special Publication, v. 254, p. 267-287.

Haughton, P.D.W., 1994, Deposits of deflected and ponded turbidity currents, Sorbas Basin, Southeast Spain: Journal of Sedimentary Research, Section A: Sedimentary Petrology and Processes, v. 64, p. 233-246.

Haughton, P.D.W., 2001, Contained turbidites used to track sea bed deformation and basin migration, Sorbas Basin, south-east Spain: Basin Research, v. 13, p. 117-139.

HOGG, C.A., DALZIEL, S.B., HUPPERT, H.E., AND IMBERGER, J., 2015, Inclined gravity currents filling basins: The influence of Reynolds number on entrainment into gravity currents: Physics of Fluids, v. 27, no. 096602.

KOMAR, P.D., 1977, Computer simulation of turbidity current flow and the study of deep-sea channels and fan sedimentation, in Goldberg, E.D., McCave, I.N., O'Brien, J.J., Steele, J.H. eds., The Sea: Ideas and Observations on Progress in the Study of the Seas, v. 6, Marine Modelling, New York, John Wiley, p. 603-621.

LAMB, M.P., HICKSON, T., MARR, J.G., SHEETS, B., PAOLA, C., AND PARKER, G., 2004, Surging versus continuous turbidity currents: Flow dynamics and deposits in an experimental intraslope minibasin: Journal of Sedimentary Research, v. 74, p. 148-155.

MACDONALD, H.A., PEAKALL, J., WIGNALL, P.B., AND BEST, J.L., 2011. Sedimentation in deep-sea lobe-elements: implications for the origin of thickening-upward sequences: Journal of the Geological Society of London, v. 168, p. 319-331.

MARINI, M., PATACCI, M., FELLETTI, F., AND MCCAFFREY, W.D., 2016, Fill to spill stratigraphic evolution of a confined turbidite mini-basin succession, and its likely well bore expression: The Castagnola Fm, NW Italy: Marine and Petroleum Geology, v. 69, p. 94-111.

MCCAFFREY, W.D. AND KNELLER, B.C., 2001, Process controls on the development of stratigraphic trap potential on the margins of confined turbidite systems and aids to reservoir evaluation: American Association of Petroleum Geologists Bulletin, v. 85, p. 971-988.

MUCK, M.T., AND UNDERWOOD, M.B., 1990, Upslope flow of turbidity currents; a comparison among field observations, theory, and laboratory models: Geology, v. 18, p. 54-57.

PATACCI, M., 2010, Termination of turbidites against confining slopes: Flow behaviour and facies trends: PhD Thesis, University College Dublin, Dublin, Eire, p. 382.

PATACCI, M., HAUGHTON, P.D., AND MCCAFFREY, W.D., 2015, Flow behavior of ponded turbidity currents: Journal of Sedimentary Research, v. 85, p. 885-902.

Pirmez, C., Prather, B.E., Mallarino, G., O'Hayer, W.W., Droxler, A.W. and Winker, C.D., 2012, Chronostratigraphy of the Brazos-Trinity depositional system, western Gulf of Mexico: Implications for deepwater depositional models, in Prather, B.E., Deptuck, M.E., Mohrig, D., Van Hoorn, B., and Wynn, R.B., eds., Application of the Principles of Seismic Geomorphology to Continental-Slope and Base-of-Slope Systems: Case Studies from Seafloor and Near-Seafloor Analogues: Society for Sedimentary Geology Special Publication, v. 99, p. 111-143.

Prather, B.E., Pirmez, C., and Winker, C.D., 2012, Stratigraphy of linked intraslope basins: Brazos-Trinity System western Gulf of Mexico, in Prather, B.E., Deptuck, M.E., Mohrig, D., Van Hoorn, B., and Wynn, R.B., eds., Application of the Principles of Seismic Geomorphology to Continental-Slope and Base-of-Slope Systems: Case Studies from Seafloor and Near-Seafloor Analogues: Society for Sedimentary Geology Special Publication, v. 99, p. 83-109.

Prelat, A. and Hodgson, D.M., 2013, The full range of turbidite bed thickness patterns in submarine lobes: controls and implications: Journal of the Geological Society of London, v. 170, p. 209-214.

Shin, J.O., Dalziel, S.B., and Linden, P.F., 2004, Gravity currents produced by lock exchange: Journal of Fluid Mechanics, v. 521, p. 1-34.

Smith, R., and Joseph, P., 2004, Onlap stratal architectures in the Gres d'Annot: geometric models and controlling factors, in Joseph, P. and Lomas, S.A. eds, Deep-Water Sedimentation in the Alpine Basin of SE France: New Perspectives on the Gres D'Annot and Related Systems: Geological Society of London, Special Publications, v. 221, p. 389-399.

Soulsby, R., 1997, Dynamics of marine sands: a manual for practical applications. Thomas Telford, London.

Spychala, Y.T., Hodgson, D.M., Stevenson, C.J., and Flint, S.S., 2017, Aggradational lobe fringes: The influence of subtle intrabasinal seabed topography on sediment gravity flow processes and lobe stacking patterns: Sedimentology, v. 64, p. 582-608.

Sylvester, Z., Cantelli, A., and Pirmez, C., 2015, Stratigraphic evolution of intraslope minibasins: Insights from surface-based model: American Association of Petroleum Geologists Bulletin, v. 99, p. 1099-1129.

Tinterri, R., and Tagliaferri, A., 2015, The syntectonic evolution of foredeep turbidites related to basin segmentation: Facies response to the increase in tectonic confinement (Marnoso-arenacea Formation, Miocene, Northern Apennines, Italy): Marine and Petroleum Geology, v. 67, p. 81-110.

Toniolo, H., Lamb, M., and Parker, G., 2006, Depositional turbidity currents in diapiric minibasins on the continental slope: Formulation and theory: Journal of Sedimentary Research, v. 76, p. 783-797.

Twichell, D.C., Cross, V.A., Hanson, A.D., Buck, B.J., Zybala, J.G., and Rudin, M.J., 2005, Seismic architecture and lithofacies of turbidites in Lake Mead (Arizona and Nevada, USA), an analogue for topographically complex basins: Journal of Sedimentary Research, v. 75, p. 134-148.

Van Andel, T.H., and Komar, P.D., 1969, Ponded sediments of the Mid-Atlantic Ridge between 22° and 23° north latitude: Geological Society of America Bulletin, v. 80, p. 1163-1190.

Xu, J.P., 2010, Normalized velocity profiles of field-measured turbidity currents: Geology, v. 38, p. 563-566.

Xu, J.P., Noble, M.A., and Rosenfeld, L.K., 2004, In-situ measurements of velocity structure within turbidity currents: Geophysical Research Letters, v. 31, no. L09311.

Table 1. Constraints on ponded cloud inflation.

Flow Type	Cloud Height	Dynamical Constraints
ia) substantial inflation	$H_d > H_r$	$q_I > A_r w_s$, $t_d \geq t_t$
ib) limited inflation	$H_t < H_d \leq H_r$	$A_t w_s < q_I \leq A_r w_s$, $t_d \geq t_t$
ii) ponding	$0 < H_d \leq H_t$	$LWw_s < q_I \leq A_t w_s$, $t_d \geq t_t$
iii) surge	n/a	$q_I \geq LWw_s$, $t_d < t_t$
iv) unconfined	n/a	$q_I < LWw_s$, $t_d < t_t$

Table 2. Empirical data sources used in Figure 3.

System		Source	Data
BR	Brazos system, Basin IV	Pirmez et al. 2012 Expedition 308 Scientists 2006	Basin Geometry Bed Thickness
CA	Castagnola, Unit 1	Felletti 2002 Marini et al. 2016	Basin Geometry Bed Thickness
CC	Congo Canyon, flows 1-11	Cooper et al. 2013	Flow Duration
GC	Gaoping Canyon, flow 1	Carter et al. 2012	Flow Duration
HC	Hueneme Canyon, event 2	Xu 2010	Flow Concentration
MA	Marnoso Arenacea, Unit III	Argnani and Ricci Lucchi 2001 Tinterri and Tagliaferri 2015	Basin Geometry Bed Thickness
MC	Monterey Canyon, event 2	Xu et al. 2004 Xu 2010	Flow Duration Flow Concentration
TS	Tabernas-Sorbas	Haughton 1994 Haughton 2001	Basin Geometry Bed Thickness

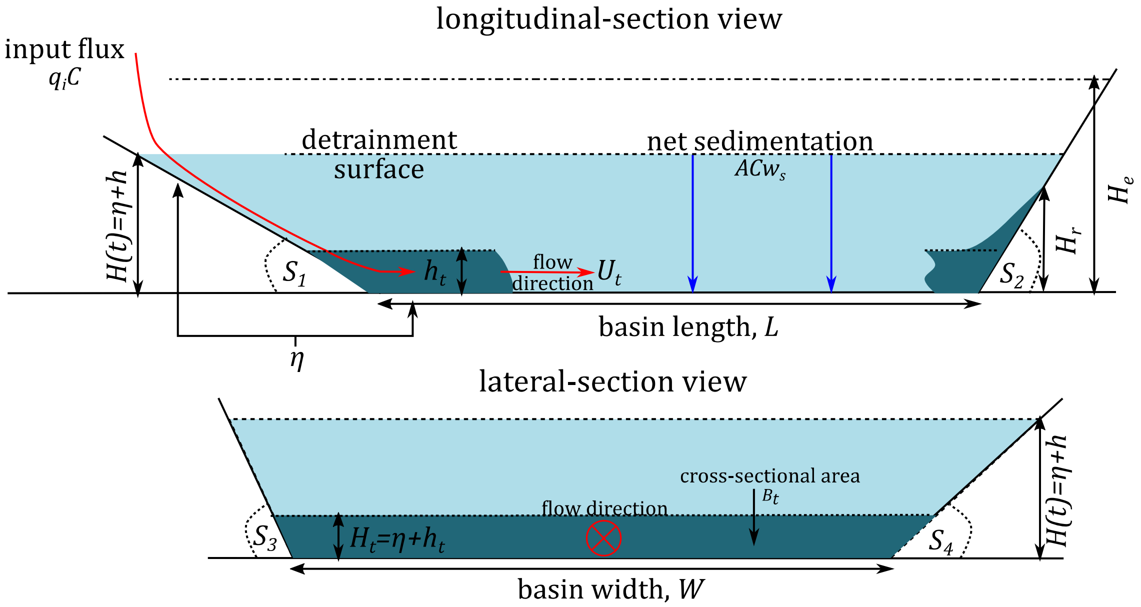

Figure 1. Schematic diagram of simplified model basin showing longitudinal and lateral-section views of the initial basin-floor flow and later ponded cloud inflation.

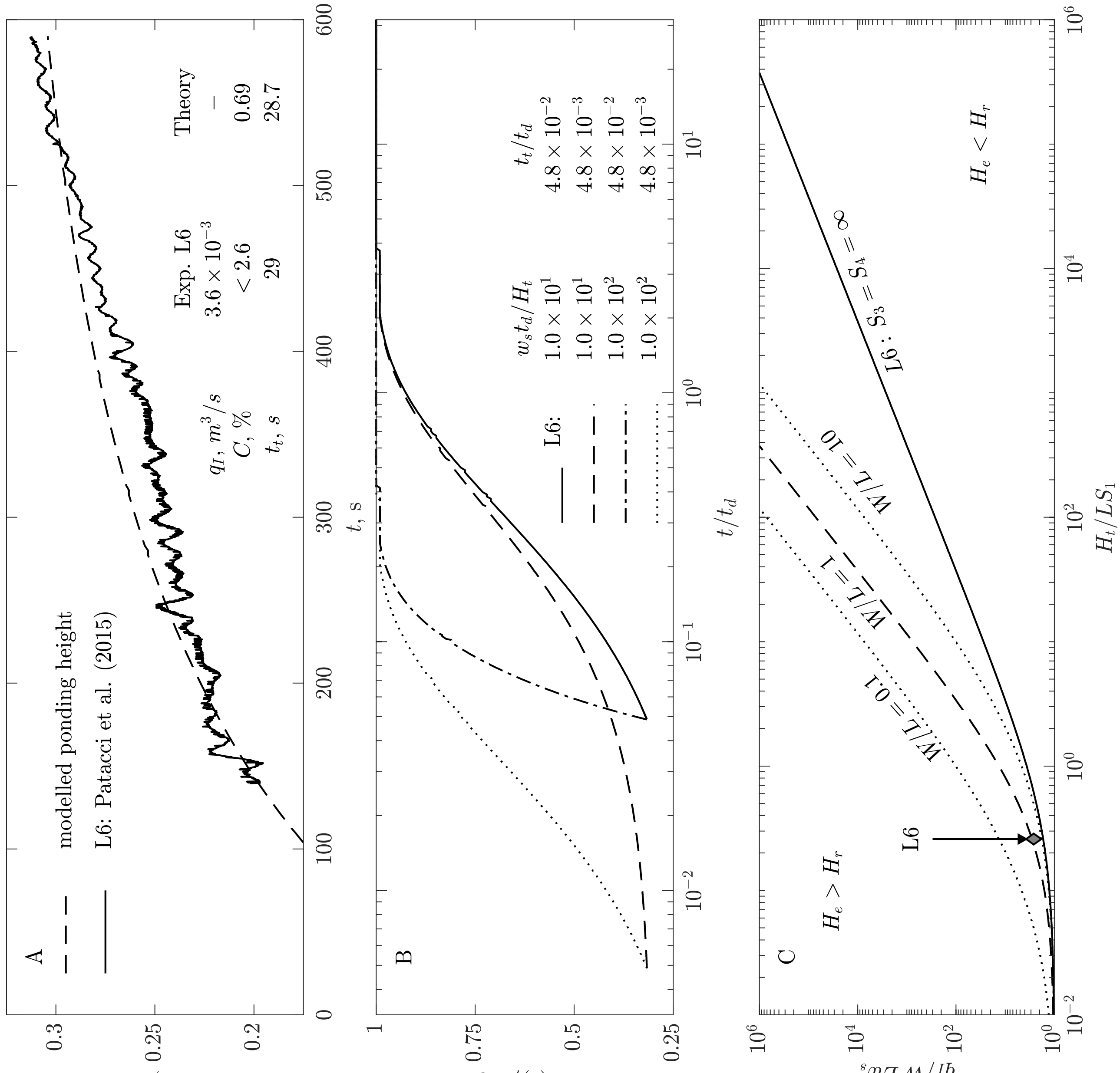

Figure 2. A) Comparison of predicted (Eq. 5) and empirical (Exp. L6: Patacci et al., 2015) measurements of inflation height of a ponded cloud. B) Dimensionless inflation rate as a function of equilibrium flow depth and flow duration . C) Criterion for inflation above flow run-up height of infinite-duration ponded flows.

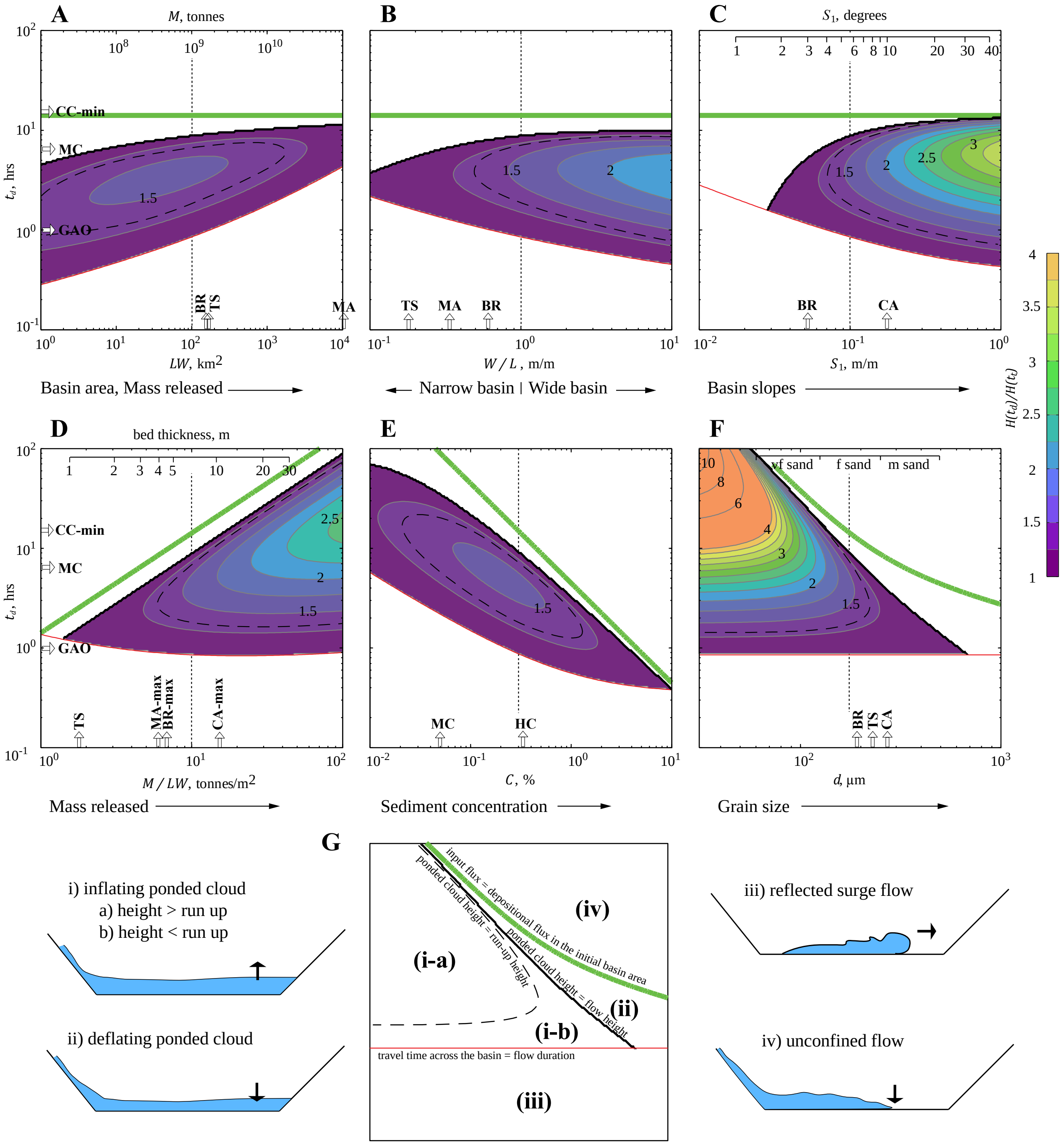

Figure 3. Phase space of the ratio of ponded cloud height to flow height as a function of flow duration and: (A) basin size; (B) width to length aspect ratio; (C) basin slope; (D) mass released; (E) flow concentration; and (F) particle diameter. Basin geometry and flow conditions kept constant across plots A-F are $LW = 100$ km^2, $W/L = 1$ m/m, $S_1 = S_2 = S_3 = S_4 = 0.1$ m/m, $M/LW = 10$ tonnes/m^2, $C = 0.3\%$ and $d = 177$ μm, whose values are shown as vertical dashed lines in parts A) to C), respectively. White arrows denote real world examples (single values or max/min values); abbreviations and data sources are shown in Table 2. Part G identifies four distinct flow regimes i-iv,

delimited by: solid black line, denoting $H_d = H_t$ (ponded-cloud height = flow height); dashed black curve, denoting $H_d = H_r$ (ponded cloud height = run-up height); thin red line, denoting t_t/t_d (travel time across the basin = flow duration); thick green line, denoting $q_I = LWw_s$ (input flux = depositional flux in the initial basin area).

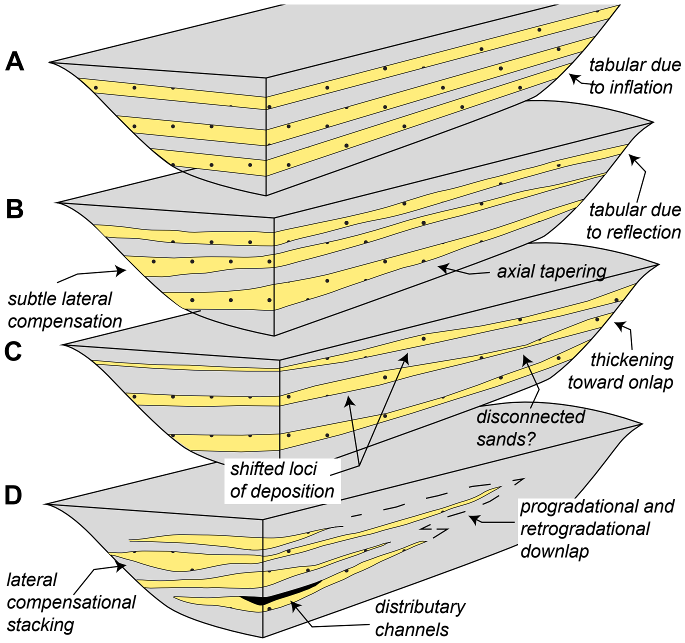

Figure 4. Idealized basin-fill architectures under the four ponding scenarios identified in Figure 3: A) Tabular beds that extend across the entire basin; B) basinwide sands that may show some degree of compensation or tapering, or that may be tabular; C) disordered deposits with shifting loci of deposition and possible disconnected sands; and D) effectively unconfined deposits showing lobe compensation and channelization.